RSC Advances

PAPER

View Article Online
View Journal | View Issue

Cite this: *RSC Adv.*, 2020, **10**, 655

Fouling analysis and permeate quality evaluation of mulberry wine in microfiltration process†

Qin-Mei Xiong,[ab] Jian Liu,[ab] Miao Liu,[c] Cai-Hong Shen,[c] Xue-Chun Yu,[d] Chong-De Wu,[ab] Jun Huang,[ab] Rong-Qing Zhou[abe] and Yao Jin*[ab]

Received 1st November 2019
Accepted 9th December 2019

DOI: 10.1039/c9ra09034g

rsc.li/rsc-advances

Sterilization and clarification are essential to produce wine of high quality and stability, microfiltration is a serious candidate for both purposes. In this work, microfiltration of fermented mulberry wine was evaluated for the first time. Four different commercial membranes, of two different materials (PES, PVDF) and two different nominal pore sizes (0.22 μm and 0.45 μm) were employed. Pore blocking model was used to identify the fouling mechanism, foulant constituents were revealed by FT-IR spectra. The effect of microfiltration on permeate quality of mulberry wine was also involved. The results indicated that cake formation was the dominant mechanism during steady-state of mulberry wine microfiltration, independently on the membrane property. The fouling layer was mainly composed of protein and polysaccharides, which induced basically reversible overall filtration resistance. Microfiltration delivered a superior clarity, highly polydisperse and light-color mulberry wine with a satisfactory sterilization stability. It preserved the main basic properties and organic acid contents of mulberry wine while resulted in certain loss of volatile compounds, especially esters and alcohols. This work has provided a scientific reference for producing mulberry wine, a modern functional beverage.

1. Introduction

Mulberry wine has been reported with multiple beneficial pharmacological effects thanks to its high content of various bioactive substances, such as organic acids, polyphenols, especially anthocyanins and resveratrol, thus becoming a modern functional beverage of interest.[1–3] In the last decades, it has been widely investigated from the perspective of yeast strain,[4,5] fermentation/aging process[1,6] and polyphenol/volatile compounds.[7,8]

The above-mentioned works have established a basic understanding for the development of mulberry wine production. However, current investigation is far from adequate to sustain a high-efficiency production of mulberry wine. The outcome of high quality mulberry wine after fermentation and aging process is reachable, the gain of a long-term stable high-quality wine is now the challenge, which requires an urgent investigation of the final process before package: sterilization and clarification.

Microfiltration is the widely used process for sterilization and clarification of grape wine and cider.[9] Not only it can provide products with superior clarity while keeping most of the flavor and nutrition substances, but also it is able to remove the microorganisms to stop the fermentation and stabilize wine. Microfiltration of grape wine has already been investigated for decades. Membrane fouling of such process has always been the main obstacle of its large-scale application.[10] The fouling build-up during wine microfiltration was reported to be mainly governed by the fine colloidal particles, referring to lyophilic macromolecules (polysaccharides), which caused severe irreversible fouling, while large particles (>2 μm) contributed to the cake formation and dominated the overall membrane resistance evolution.[11] The adsorption of polyphenolic compounds originating from wine was also showed to impact the microfiltration performance, due to fouling resulting from the interaction between polyphenols and the membrane surface.[14]

Such works on grape wine have provided a solid reference to explore the process of mulberry wine microfiltration. However, they can not offer direct guiding information for mulberry wine production, after all, different raw fermentation feeds (fruits) exhibited diverged properties which may result in unexpectedly different outcomes. Both grape fruits and mulberry fruits are excellent sources of polyphenols,[15] but they are quite different in terms of bioactive compounds and mineral composition,[16–18] making the dedicated investigation on mulberry wine microfiltration necessary. Moreover, membrane fouling is a complex outcome of feed characteristics,[12,19] membrane properties[13,20]

[a]College of Biomass Science and Engineering, Sichuan University, Chengdu 610065, China. E-mail: yaojin12@scu.edu.cn; Fax: +86-28-85405237; Tel: +86-138-8219-7633
[b]Key Laboratory for Leather and Engineering of the Education Ministry, Sichuan University, Chengdu 610065, China
[c]Lu Zhou Lao Jiao Co.,Ltd, Luzhou 646000, China
[d]Luzhou Pinchuang Technology CO.,LTD, Luzhou 646000, China
[e]National Engineering Research Center of Solid-State Manufacturing, Luzhou 646000, China

† Electronic supplementary information (ESI) available. See DOI: 10.1039/c9ra09034g

and operating conditions,[21] which necessitates a particular attention of research work.

Therefore, the aim of this work was to provide a guidance for the process of mulberry wine microfiltration, by analyzing the microfiltration performance with different membranes, then relating to the pore blocking mechanism and foulant identification. This work also explored the effect of microfiltration on the quality of mulberry wine, for the sake of delivering a multi-aspect evaluation of such process. From the best of our knowledge, this is the first time that microfiltration of mulberry wine is being evaluated, which is expected to contribute to the foundation build-up for further development of such process and reference for relevant research.

2. Materials and methods

2.1 Wine preparation and chemicals

Ripe mulberry fruits (*Morus notabilis* C. K. Schneid) were purchased from local supplier in Sichuan province (China). 60 ppm of SO_2 was added into the crushed fruits to inhibit bacteria growth and prevent oxidation. After the adjustment of nitrogenous and carbonate source, two types of commercial yeasts (Zymaflore Alpha, Lalvin D254) were added to initiate fermentation, which then lasted 8 days under 25 °C in a stainless fermenter. When the alcohol content reached 12% v/v and the residual sugar dropped to 2%, the pomace was removed to conduct secondary fermentation for another 10 days under 17 °C. Subsequently, the ferment was filtrated by cheesecloth and then stabilized in the darkness at 2 °C for 15 days. The mulberry wine involved in this study was then sampled after this process, involving two kinds of samples: the immediately sampled one after stabilization referred to samples of natural clarification, the others referred to the permeate of microfiltration.

All chemical reagents used in this study were purchased from Sigma-Aldrich (St. Louis, Mo, USA) and Aladdin (Shanghai, China); they were of analytical grade.

2.2 Experimental set-up and procedure

Four sheet membranes with pore sizes of 0.22 μm and 0.45 μm, made of polyethersulfone (PES, Millipore, Co. Ltd., USA) and polyvinylidene fluoride (PVDF, Millipore, Co. Ltd., USA) were used in this study. The specific membrane properties are shown in Table 1. The membrane surface porosity was determined by analyzing the scanning electron microscope (SEM) images with the software Image-Pro Plus (version 6.0, Media Cybernetics, Co. Ltd., America). The hydrophilicity of the membrane was expressed by the contact angle measured by a Video based contact angle measuring device (OCAH200, DataPhysics, Co. Ltd., Germany). Prior to use, all the membranes were soaked in water for 24 hours to remove impurities or additives from the fabrication process.

Mulberry wine samples were microfiltered under a trans-membrane pressure (ΔP) of 0.06 MPa at ambient temperature (25 ± 1 °C), with the four above-mentioned flat membranes by a commercial stirred (300 rpm) dean-end filtration cell (Millipore, Co. Ltd., USA). Preliminary experiments were conducted to determine the optimal operating conditions mentioned above. The pressure was applied *via* purified compressed air and was monitored by pressure gauges. The permeate was monitored by a reservoir placed on a digital balance with an accuracy of 0.01 g which was connected to a computer by measuring the mass variation in a reservoir vessel every one minute Fig. 1 illustrates a simplified scheme of the dead-end microfiltration set-up.

At the beginning and at the end of each microfiltration run, permeate flux of distilled water was measured at $\Delta P = 0.06$ MPa, in order to monitor the change of water permeability of membrane after mulberry wine microfiltration.

2.3 Models of membrane fouling analysis

2.3.1 Resistance-in-series model. Resistance-in-series model is the classical model and it was already applied in our previous work.[22] The permeate flux through the membrane can be calculated in accordance with Darcy's law (eqn (1)):

$$J = \frac{\Delta P}{\mu R_t} \quad (1)$$

where J is the permeate flux ($m^3\ m^{-2}\ s^{-1}$), ΔP is the trans-membrane pressure (Pa), μ is the dynamic viscosity of the permeate (Pa s), and R_t is the total resistance to the filtration process (m^{-1}). Shown in (eqn (2)):

$$R_t = R_m + R_f = R_m + R_c + R_{cp} + R_{irrf} \quad (2)$$

where R_m is new membrane resistance (m^{-1}), R_f is the fouling resistance formed during microfiltration (m^{-1}), R_c and R_{cp} are respectively caused by filter cake contamination and concentration polarization on membrane surface, which can be removed by simple cleaning. On the contrary, R_{irrf} is caused by membrane pore blockage and material adsorption, which is difficult to remove by simple cleaning.

R_m and R_t can be calculated by the following formula (eqn (3) and (4)):

Table 1 Intrinsic properties of employed membranes

Material	Module	Filtration area	Pore size (μm)	Porosity (%)	Contact angle (°)	Denote
PES	Flat sheet	0.0045 m^2	0.22	28.97 ± 2.90	44.2 ± 0.3	PES0.22
PES			0.45	43.75 ± 2.64	52.7 ± 0.0	PES0.45
PVDF			0.22	34.82 ± 3.91	63.5 ± 0.6	PVDF0.22
PVDF			0.45	42.77 ± 1.17	82.1 ± 0.4	PVDF0.45

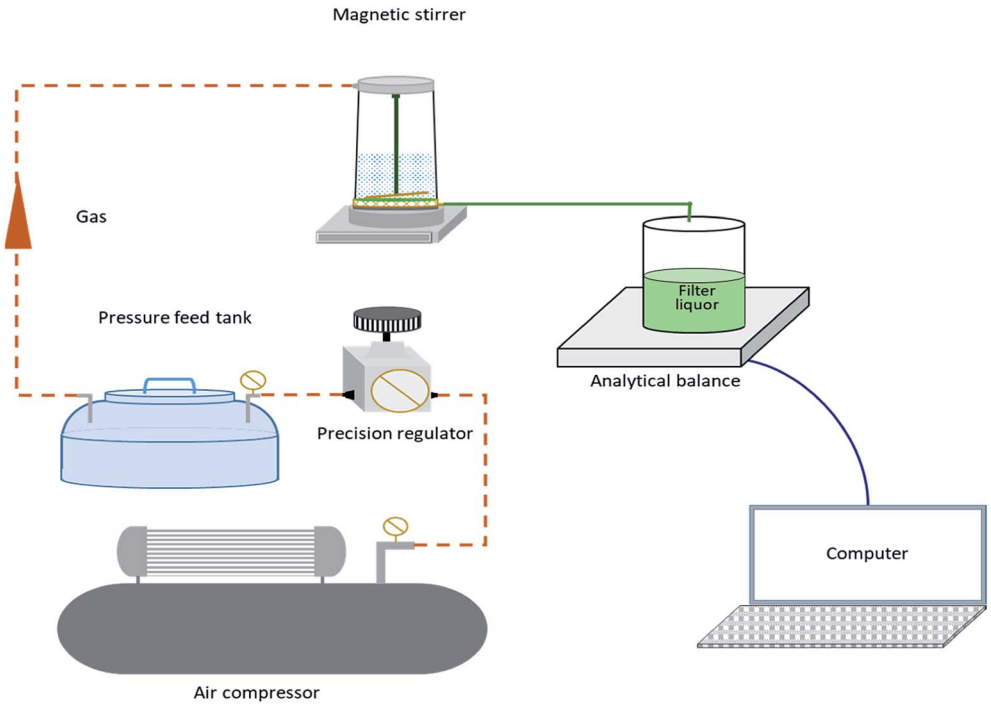

Fig. 1 Schematic diagram of the laboratory set-up.

$$R_m = \frac{\Delta P}{\mu_0 J_0} \quad (3)$$

$$R_t = \frac{\Delta P}{\mu_t J_t} \quad (4)$$

where $\mu_0 = 0.894 \times 10^{-3}$ Pa s, which is the viscosity of water at 25 °C, and J_0 is the pure water flux before microfiltration; $\mu_t = 1.76 \times 10^{-3}$ Pa s, which is the viscosity of mulberry wine, it was measured by rheometer (DHR-1, TA Instrument, Co. Ltd., America) at 25 °C. And J_t is the permeate flux at steady state ($m^3\ m^{-2}\ s^{-1}$).

After the microfiltration, the remaining sample inside the filtration cell was gently poured out, then pure water was added to refill the cell, the steady-state permeate flux was measured again at this stage, denoted as J_1. Afterwards, the filtration cell and membrane were finally washed with plenty of water, a final water flux was measured, denoted as J_2. With the help of J_1 and J_2, R_c, R_{cp} and R_{irrf} can be estimated by the following formula:

$$R_{irrf} = \frac{\Delta P}{\mu_0 J_2} - \frac{\Delta P}{\mu_0 J_0} \quad (5)$$

$$R_{cp} = \frac{\Delta P}{\mu_t J_t} - \frac{\Delta P}{\mu_0 J_1} \quad (6)$$

$$R_c = R_t - R_m - R_{cp} - R_{irrf} = \frac{\Delta P}{\mu_0 J_1} - \frac{\Delta P}{\mu_0 J_2} \quad (7)$$

2.3.2 Pore blocking model. The fouling mechanism was analyzed by using the derivations of pore blocking model proposed by Hermans and Bredee, which is now widely used to describe classical dead-end filtration:[23–26]

Complete pore blocking:

$$j = e^{-\alpha_b t} \quad (8)$$

Internal pore constriction blocking:

$$j = (1 + 2\alpha_i t)^{-2} \quad (9)$$

Cake filtration:

$$j = (1 + 2\alpha_c t)^{-0.5} \quad (10)$$

where j is the relative flux $\left(j = \frac{J}{j_0}\right)$, t indicates the filtration time (s), j_0 is the initial flux ($L\ m^{-2}\ h^{-1}$). α_b is the system parameter relating to complete pore blocking (s^{-1}), α_i is the system parameter relating to internal pore constriction blocking (s^{-1}), α_c is the system parameter relating to cake filtration (s^{-1}).

2.4 Analytical methods

2.4.1 Basic properties of wine samples. Turbidity was determined by a turbidity meter (WZS-186, Lei-ci, Co. Ltd., Shanghai, China), the particle size distribution was determined by granulometer (ZN3600+ MTP2, Malvern, Co. Ltd., Shanghai, China). Chromaticity was determined by a double-beam UV-visible spectrophotometer (L7, Shang-fen, Co. Ltd., Shanghai, China) and pH was determined by a pH meter (DZS-708-A, Lei-ci, Co. Ltd., Shanghai China). The soluble solid content was determined by a Hand-held refractometer (IR240, Insmark, Co. Ltd., Shanghai, China). Alcoholic strength, total sugar and total

acid were examined by the laboratory according to the National Standard of the People Republic of China (GB/15038-2006). The total phenols were determined by Folin–Ciocalteu's method,[27] the results were expressed as equivalent gallic acid (g gallic acid/L). In order to characterize the long-term stability of the mulberry wine during storage, the total bacteria count was taken as the main indicator to carry out the temperature acceleration shelf-life test at 37 °C for 40 days. Each sample was repeated in triplicate to ensure good repeatability.[28]

2.4.2 Organic acid of wine samples. The analytical method for organic acid in mulberry wine was based on our previously-defined protocol.[29] The samples were diluted appropriately, centrifuged for 10 min, then purified with a C_{18} SPE column (Swell Scientific Instrument. Co. Ltd., Chengdu, China) before HPLC analysis. The prepared 9.00 mM H_2SO_4 was degassed for 30 min before it was used as the mobile phase. Six sets of organic acid standards including citric acid, tartaric acid, malic acid, lactic acid, acetic acids, and succinic acid were applied to HPLC analysis to establish the calibration curves in order to implement the quantitative detection of organic acids in mulberry wine samples.

A single sample of 20 μL was then injected into an Agilent 1260 HPLC system equipped with an Alltech OA-1000 organic acid column (300 × 78 mm) maintained at 75 °C with UV detector (210 nm). All samples were measured in triplicate.

2.4.3 Volatile compounds of wine samples. The analytical method for volatile compounds in mulberry was based on our previously-defined protocol with modification.[29–31] Accurately measured 0.5 mL of wine sample and 1.5 g NaCl were added into the 20 mL headspace vials with a Teflon cover to promote the volatilization of volatile components. A volume of 10 μl methyl octanoate solution (0.051 g L^{-1}) was added into the headspace vial as internal standard. The samples were pre-equilibrated at 60 ± 1 °C in a thermostatic bath for 15 min, then a 50/30 μm DVB/CAR/PDMS fiber (Supelco, Inc., Bellefonte, PA, USA) was inserted and exposed in the upper space for another 40 min to absorb the volatiles.

GC-MS apparatus (Trace GC Ultra gas chromatograph-DSQ II mass spectrometer, Thermo Electron Corporation, Waltham, America) equipped with an HP-INNOWAX capillary column (30.0 m × 0.25 mm × 0.25 μm, Agilent Technology, Santa, USA) was used to separate and detect the volatile components of the mulberry wine samples. The injector temperature was set to 250 °C, high purity helium gas (99.999%) with a flow rate of 1.00 mL min^{-1} was used as the carrier gas. The split mode was used and the ratio was 10 : 1. Then oven temperature was programmed as follows: the initial temperature was 40 °C for 5 min, then ramped at 4 °C min^{-1} to 100 °C and then 6 °C min^{-1} to 220 °C for 8 min. The mass spectrum was operated in the positive ion electron impact ionization (EI+) mode at 70 eV in a range of 35–400 amu. The temperature of the ion source and transfer line were set at 230 °C and 250 °C, respectively.

The identification and retention index of each volatile were respectively obtained by comparing their mass spectrum with the NIST05 library database (Finnigan Co. Ltd., California, USA). The relative content of each volatile was then determined by the ratio between the peak area of the specific compound and that of the internal standard. All samples were analyzed in triplicate and the results were noted as the mean value ± relative standard deviation (RSD).

2.4.4 Membrane morphology and fouling analysis. The microscopical morphology of pristine/fouled membrane as well as the functional groups of foulant layer were evidenced by SEM and ATR-FTIR analysis. Both surface and cross section of the new, fouled and cleaned (by pure water) membrane were demonstrated by a scanning electron microscopy (JSM-6510LV, JEOL, Japan). Before SEM analysis, the air-dried membrane samples were carefully pasted on the conductive glue and sprayed with a golden layer. As for cross-section observation, the membrane samples were firstly immersed in liquid nitrogen and then certain fractures of membrane were selected to continue with sticking and spraying treatment. The presence of specific functional groups on the air-dried membrane surface was analyzed by ATR-FTIR (Nicolet IS10, Co. Ltd., Thermo Scientific, America).

2.4.5 Statistical analysis. Triplicate experiments were conducted on each sample and the data was represented in the form of mean relative standard deviation (RSD). One-way ANOVA was conducted using SPSS software (version 17.0; SPSS Inc., Chicago, IL, USA) to complete the significant difference test, at significant level of $P < 0.05$. Three different batches ($n = 3$) were considered and analyzed throughout the study.

3. Results and discussion

3.1 Microfiltration performance

Fig. 2 shows the evolution of permeate flux over time during the whole microfiltration process for different membranes. Basically, a quick and dramatic decline occurred during microfiltration, with whichever membrane. The membranes with bigger nominal pore size (0.45 μm) showed higher permeate flux at the early stage of process, which then progressively declined into the same flux level to the membranes with smaller nominal pore size (0.2 μm). Among the tested membranes, PVDF0.45 showed the highest steady-state permeate flux.

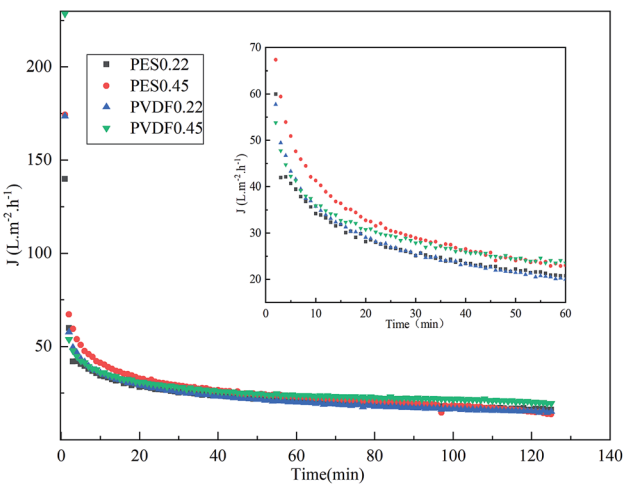

Fig. 2 Permeate flux over time in mulberry wine microfiltration.

Table 2 Decomposition of fouling resistance in mulberry wine microfiltration

	Microfiltration resistance (m^{-1})				
Membranes	$R_t \times 10^{12}$	$R_m \times 10^{10}$	$R_{irrf} \times 10^{9}$	$R_c \times 10^{12}$	$R_{cp} \times 10^{12}$
PES0.22	7.59	5.63	7.07	6.26	1.32
PES0.45	8.17	5.44	4.73	4.95	3.22
PVDF0.22	8.03	9.09	7.51	6.81	4.33
PVDF0.45	8.59	5.44	1.55	6.79	1.78

Table 2 decomposes the steady-state fouling resistance for each membrane at $\Delta P = 0.06$ MPa according to resistance-in-series model, incorporated in eqn (3)–(7). The total resistances (R_t) after microfiltration were quite comparable among the tested membranes, around 8×10^{12} m^{-1}, which were mainly composed of reversible fouling (R_c and R_{cp}) accounting for more than 98% of the total resistance, among which the cake resistance (R_c) was higher than concentration polarization resistance (R_{cp}). It indicates that the cake formation may be the main mechanism during microfiltration of mulberry wine. It is also noticeable that the irreversible fouling resistance (R_{irrf}) was more severe in the case of 0.22 μm than 0.45 μm, independently on the membrane materials.

3.2 Pore blocking mechanism

In order to further explore the fouling mechanism of mulberry wine microfiltration, pore blocking model was employed. Fig. 3 illustrates the fitting results of different pore blocking model derivations on the filtration data according to eqn (8)–(10). The model rate constants and regression coefficients are summarized in Table 3. All the experiments were carried out at the same operating conditions. Regarding the regression coefficients R and comparison between the fitted lines and the experimental data shown in and Table 3, cake filtration model fitted well the experimental data with no matter which membrane. Otherwise, neither complete blocking nor pore constriction could describe the fouling mechanism of mulberry wine microfiltration since the regression coefficients were too low for both. It is also noticeable that the filtration data of early stage did not perfectly fit into the three applied models, implying that the mechanism at this stage of microfiltration needed further dedicated investigation.

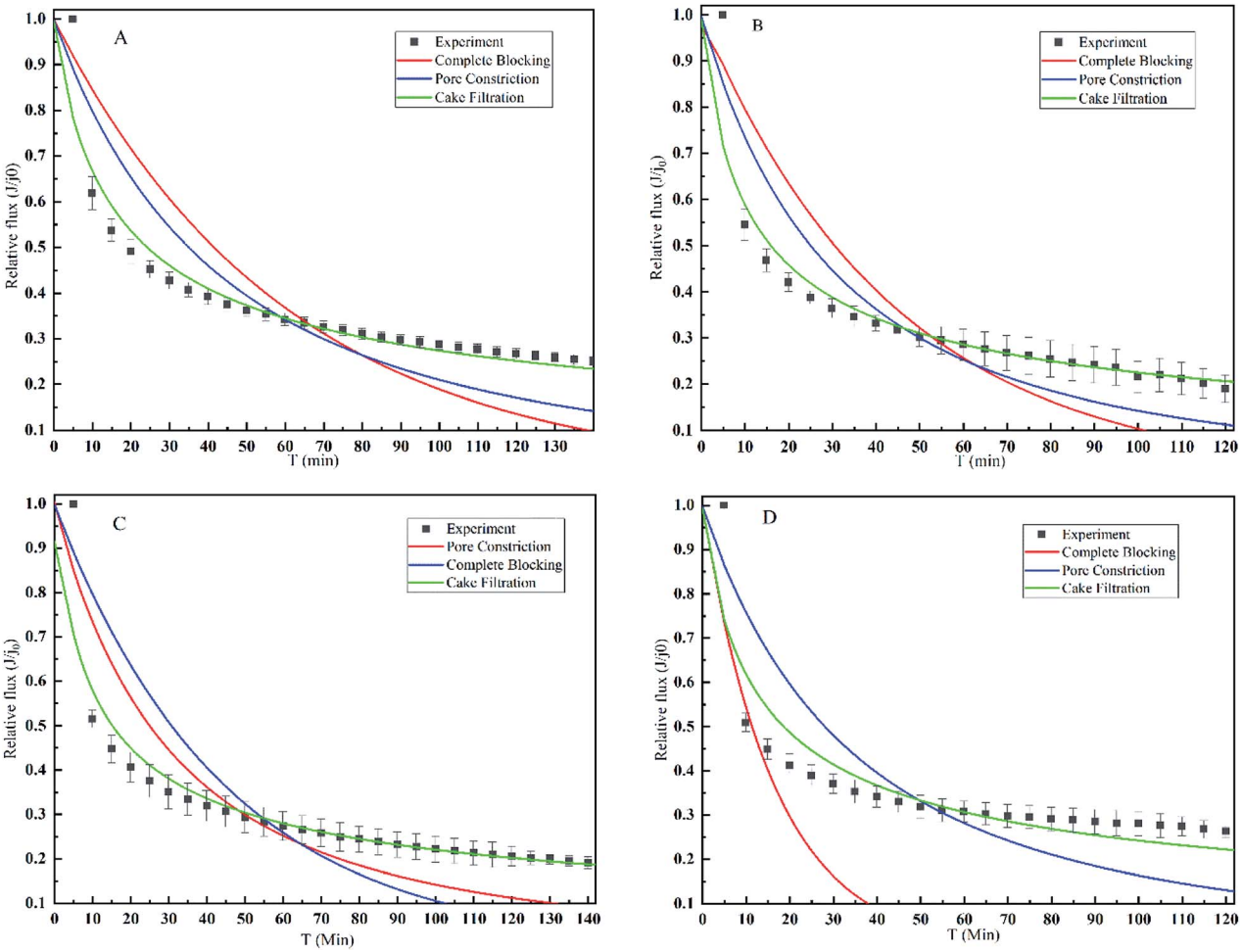

Fig. 3 Flux reduction and model fitting of mulberry wine for four different membranes: (A) PES0.22; (B) PES0.45; (C) PVDF0.22; (D) PVDF0.45. Different letters indicate that they are significantly different at $p < 0.05$ according to ANOVA analysis.

Table 3 Model rate constants and regression coefficients (R) of flux decline by different fouling models for different membranes

	Blocking		Constriction		Cake	
Membrane (nm)	α_b (min^{-1})	R	α_p (min^{-1})	R	α_c (min^{-1})	R
PES0.22	0.01663	0.5039	0.0059	0.7717	0.06165	0.9511
PES0.45	0.02316	0.635	0.00836	0.8319	0.09215	0.9304
PVDF0.22	0.02249	0.4764	0.00826	0.7772	0.098	0.9281
PVDF.45	0.06039	—	0.00735	0.582	0.07995	0.8877

Such results confirmed the suggestion of resistance-in-series model, revealed that the dominant fouling mechanism during microfiltration of mulberry wine in steady-state was indeed cake deposition, which was barely impacted by the membrane property.

3.3 Foulant identification

ATR-FTIR and SEM were employed to identify the foulants on the membrane. Fig. 4 shows the FTIR spectra and corresponding band vibration of the pristine, fouled and cleaned membranes of PVDF0.45. As shown in this figure, all the membranes showed the same spectral characteristics of a PVDF at 834 cm^{-1}, 879 cm^{-1}, 1072 cm^{-1}, 1176 cm^{-1}, 1236 cm^{-1}, 1402 cm^{-1}, which correspond to CH_2 rocking, C–C asymmetric stretching, CF_2 symmetric stretching, CF out of plane deformation, and CH_2 wagging, respectively.[32] This signifies that the intrinsic characteristics of membrane did not alter after fouling. The main difference between the fouled membrane and the others (new and cleaned) was the peaks of 1601 cm^{-1} and 3350 cm^{-1}, corresponding to the characteristic peaks of peptide bond in proteins and polysaccharides according to previous reports.[33] Such results indicate that the organic foulant of protein and polysaccharides was the major foulant compounds on/in the membrane.

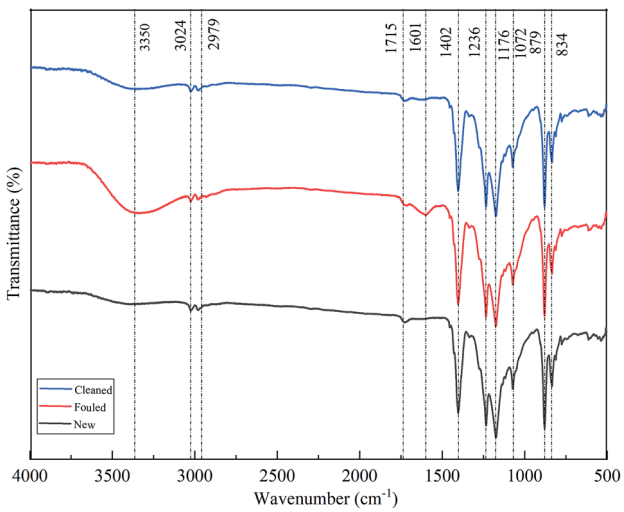

Fig. 4 ATR-FITR spectra of PVDF0.45 membrane under different conditions.

The microstructure of the membrane was evidenced by SEM. Fig. 6a and b shows the microstructure of the pristine membrane, with open membrane surface and no dirt. After microfiltration of mulberry wine, layered deposits appeared on the membrane surface (Fig. 5c) so that the membrane pores were sheltered. The cleaned membrane (Fig. 5e and f) again showed similar morphology to the pristine one, indicating an effective cleaning. The cross-section morphology of membranes then revealed the gross thickness of this deposit. As can be seen from Fig. 5b, d and f, the morphologies of the pristine and the cleaned membrane show a visualized coincidence indicating a non-deposition structure, while the fouled one was covered with a deposit of around 10 μm.

Combined the results of ATR-FTIR and SEM, one can claim that a deposit of 10 μm (dry), consisting of protein and polysaccharides, would form on the membrane surface during microfiltration of mulberry wine, and such deposit was supposed to be reversible, since pure water cleaning already showed a good efficiency to remove it.

3.4 Permeate quality

In this section, effect of microfiltration on the permeate quality of mulberry wine samples was investigated, focusing on the physicochemical properties, organic acids, volatile compounds and storing stability. A sample subjected to natural clarification was also involved in this part to provide comparative reference to the microfiltrated samples.

3.4.1 Physicochemical properties. Table 4 summarized the main physicochemical properties of mulberry wine samples. In terms of alcoholic strength, total sugar, total acid, pH, TSS, there were few differences among mulberry wine samples. Microfiltration resulted in a slight reduction of chroma and total phenol, and a dramatical decline of turbidity, from 372 NTU to <2 NTU, suggesting an effective particle removal by microfiltration. Particle size distribution of the samples further confirmed that the micron-size particles were removed and the mean particle size was significantly reduced after microfiltration (Table 4). The change of polydispersity index (PDI) also suggested that microfiltration had turned the mulberry wine samples from monodisperse (PDI = 0.26) towards polydisperse (PDI > 0.5). Such statement was illustrated in Fig. 6, the microfiltrated samples showed higher magnitude of polydispersity than the natural clarified one, for which a typical unimodal distribution was observed. Moreover, distinctions of membranes were revealed: the membranes of 0.22 μm delivered

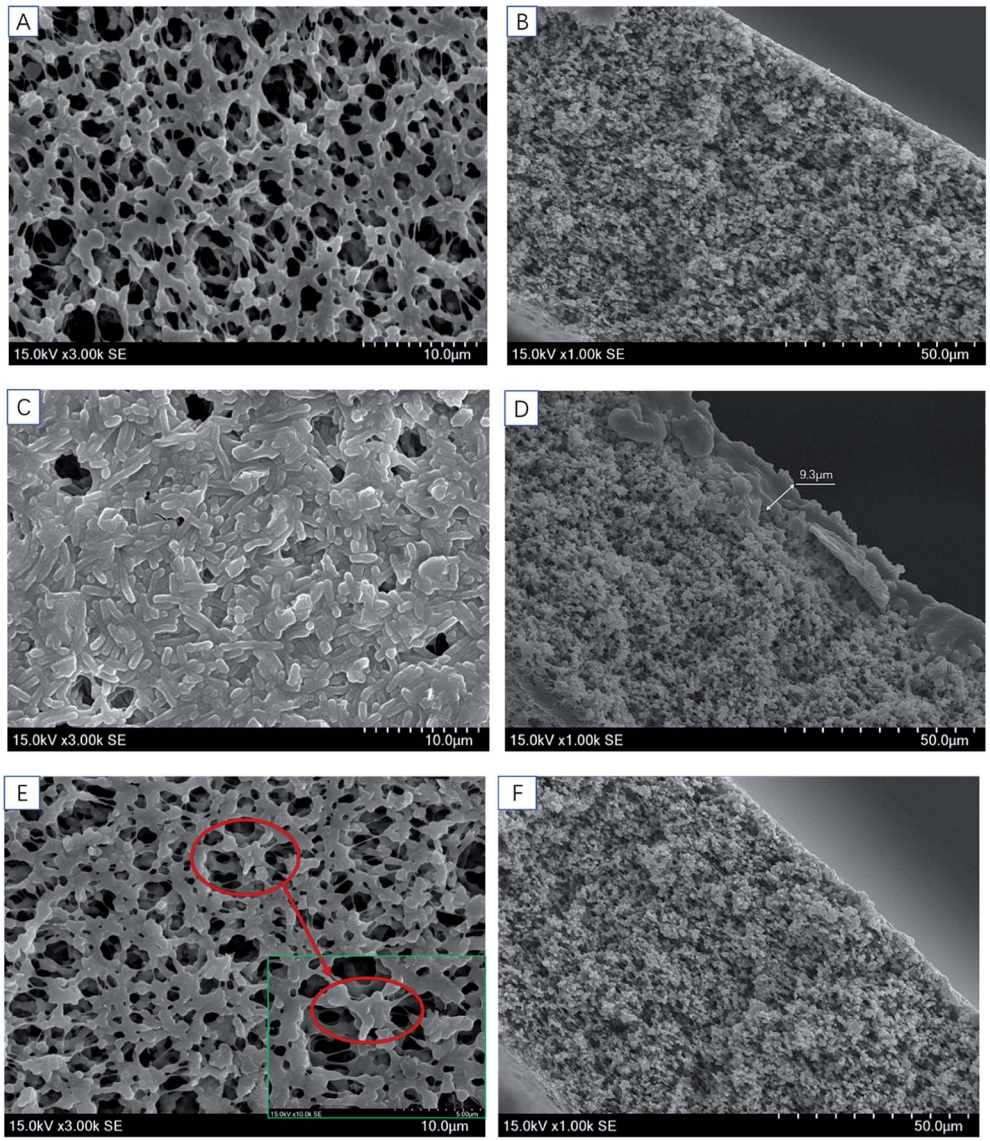

Fig. 5 SEM images of PVDF0.45: (A) surface morphology of pristine membrane (×3000) (B) cross section of pristine membrane (×1000) (C) surface of the fouled membrane (×3000) (D) cross section of the fouled membrane (×1000) (E) surface of the cleaned membrane (×3000) (F) cross section of the cleaned membrane (×1000).

Table 4 Physicochemical properties of different mulberry wine samples[a]

Parameters	Natural clarification	PES0.22	PES0.45	PVDF0.22	PVDF0.45
Alcoholic strength (V/V%)	12.8	12.4	12.8	12.5	12.7
Total sugar (g/100 mL)	2.95 ± 0.01^{b}	2.98 ± 0.00^{a}	2.92 ± 0.10^{a}	2.96 ± 0.02^{a}	2.99 ± 0.03^{a}
Total acid (g L^{-1})	10.86 ± 0.05^{a}	10.59 ± 0.06^{b}	10.68 ± 0.06^{b}	10.22 ± 0.01^{c}	10.71 ± 0.11^{b}
pH	4.87 ± 0.01^{a}	4.83 ± 0.01^{b}	4.83 ± 0.01^{b}	4.83 ± 0.01^{b}	4.87 ± 0.01^{a}
TSS (°Brix)	11.93 ± 0.06^{a}	11.90 ± 0.00^{a}	11.80 ± 0.00^{b}	11.90 ± 0.00^{a}	11.80 ± 0.00^{b}
Turbidity (NTU)	372.00 ± 2.65^{a}	1.31 ± 0.06^{b}	1.41 ± 0.02^{b}	1.26 ± 0.03^{b}	1.30 ± 0.05^{b}
Chroma	3.185 ± 0.046^{a}	2.553 ± 0.026^{c}	2.644 ± 0.038^{b}	2.564 ± 0.030^{c}	2.594 ± 0.030^{bc}
Total phenol (g L^{-1})	6.21 ± 0.02^{a}	6.02 ± 0.02^{d}	6.07 ± 0.02^{bc}	6.03 ± 0.03^{cd}	6.08 ± 0.03^{b}
Particle mean size (nm)	2350 ± 152.88^{a}	15.02 ± 2.91^{b}	54.81 ± 14.90^{b}	17.58 ± 0.98^{b}	29.20 ± 1.68^{b}
PDI	0.26 ± 0.06^{c}	0.59 ± 0.03^{b}	0.92 ± 0.13^{a}	0.60 ± 0.04^{b}	0.83 ± 0.07^{a}

[a] Mean values in the same row with different superscripted letters indicate that they are significantly different at $p < 0.05$. ANOVA analysis was applied.

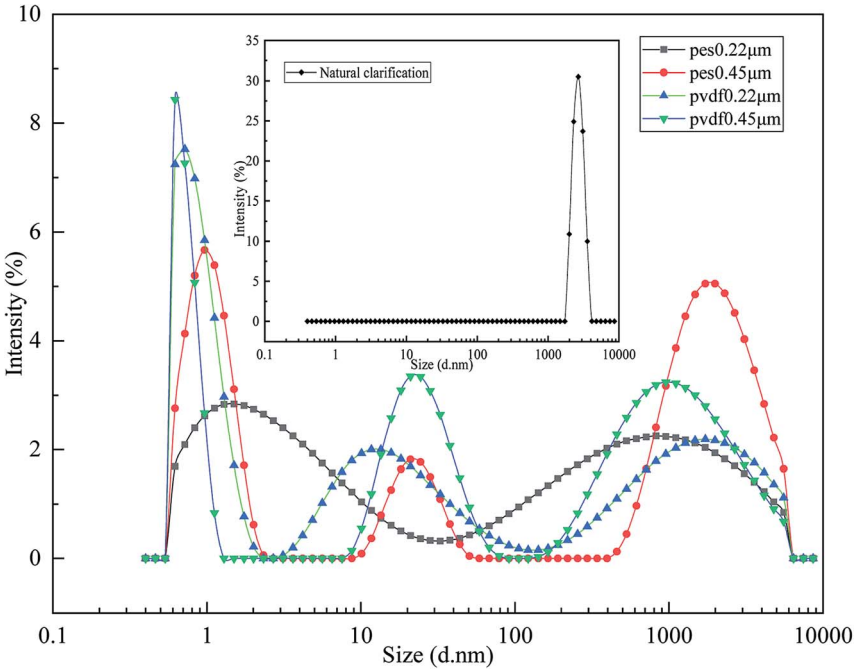

Fig. 6 Particle size distribution of mulberry wine samples.

the samples of smaller particle mean size and lower polydispersity than 0.45 μm, consistent with the expectation of sieving.

3.4.2 Organic acids. The organic acid standard solutions of 6 different concentration gradients were tested and the calibration curve of each organic acid standard was established based on the concentration and peak area. The linear correlation coefficient (R^2) for each calibration curve was greater than 0.999 (not showed), which validated the reliability of the HPLC analysis for organic acids detection.[34] As demonstrated in Fig. 7,

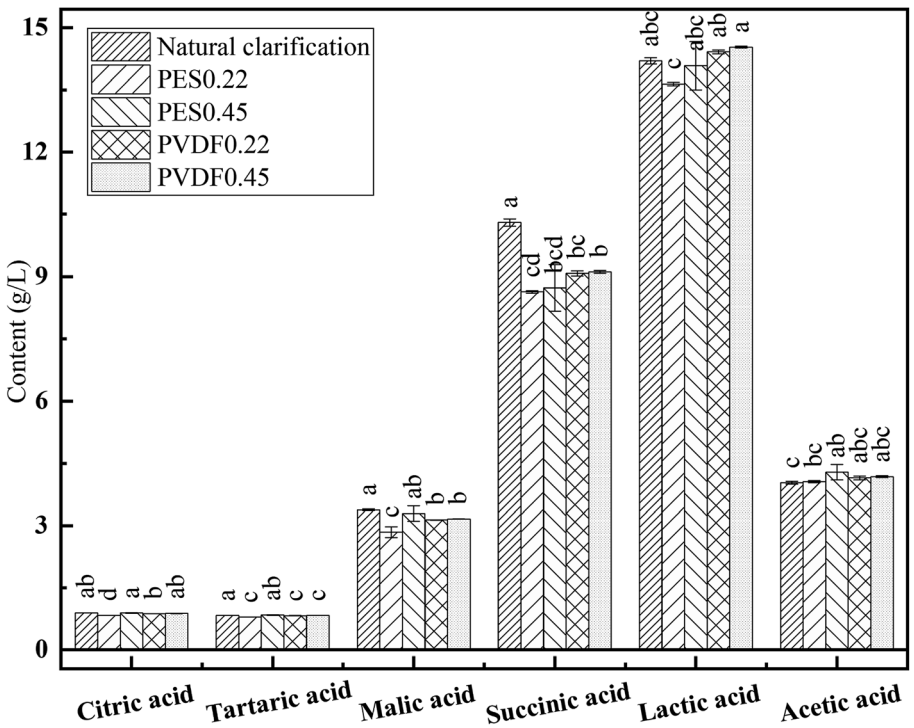

Fig. 7 The organic acid content of mulberry wine samples. Different letters indicate that they are significantly different at $p < 0.05$ according to ANOVA analysis.

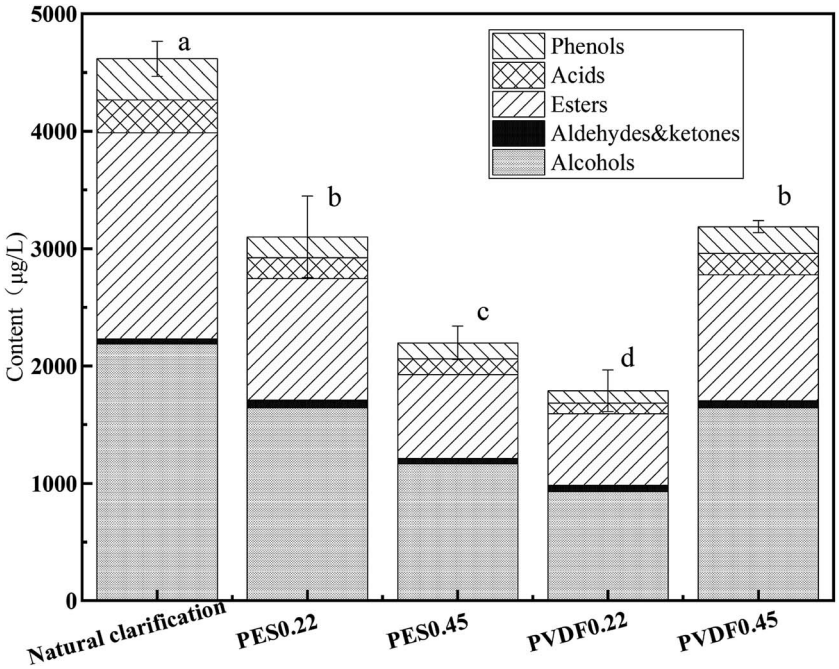

Fig. 8 Concentration/proportion of volatile compounds in mulberry wine samples. Different letters indicate that they are significantly different at $p < 0.05$ according to ANOVA analysis.

lactic acid was the most abundant organic acid in the samples, implying that a malolactic fermentation occurred during winemaking.[35] A slight content decline was revealed for malic acid, succinic acid after microfiltration. Generally, the treatment of microfiltration did not lead to sharp content declines of the 6 involved organic acids for mulberry wine samples. All the 4 involved membranes showed a fairly good capacity of organic acid preservation of mulberry wine, few distinctions among them can be remarked.

3.4.3 Volatile compounds. HS-SPME-GC-MS were used to detect the volatile compounds of mulberry wine samples. A total of 58 substances were identified and clustered into 6 groups according to the chemical structure, including 11 alcohols, 5 aldehydes and ketones, 9 acids, 28 esters and 5 phenols (Table S1†).

Fig. 8 illustrates the content and proportion of 6 volatile groups in different mulberry samples. Esters and alcohols were the dominant volatile compounds in mulberry wine samples, accounting for more than 85% of the total volatile compounds. The most abundant volatile compounds found in these mulberry wine samples were: 3-methyl-1-butanol, phenethyl alcohol, butanedioic acid diethyl ester and eugenol, with concentration superior to 300 μg L^{-1} (Table S1†). These compounds contributed a great deal to the characteristic aroma of mulberry wine, consistent with the previous reports in the literature.[5,36] After microfiltration, the content of total volatile compounds of mulberry wine samples declined to certain extent, especially for esters, alcohols and phenols. Among the 4 tested membranes, PVDF0.45 performed the best in terms of volatile compound preservation, PES0.22 also delivered a fairly good performance. Interestingly, the four tested membranes, of different materials and nominal pore sizes, did not show a convergent trend: the volatile compound preservation performance of them followed a scattered order (PVDF0.45 > PES0.22 > PES0.45 > PVDF0.22), the retention ratio of volatile compounds by membranes seemed to neither depend on the membrane material type nor the nominal pore size, but the combination of both.

3.4.4 Sterilization stability. An important role of microfiltration is to sterilize wine. Sterilization stability of the

Table 5 Stability analysis of storage life of mulberry wine samples

Parameters	Date	Natural clarification	PES0.22	PES0.45	PVDF0.22	PVDF0.45
Total bacteria (CFU mL^{-1})	d0	140	<1	<1	<1	<1
	d10	1.68×10^5	<1	<1	<1	<1
	d20	3.70×10^5	<1	<1	<1	<1
	d30	6.62×10^5	<1	<1	<1	<1
	d40	1.2×10^6	<1	<1	<1	<1
Total yeast (CFU mL^{-1})	d0	2000	<1	<1	<1	<1

mulberry wine permeate was then tracked by an accelerated storage-life test at 37 °C during 40 days in this study. As showed in Table 5, the total bacteria count of the natural clarified sample increased progressively from 140 CFU mL^{-1} to 1.2×10^6 CFU mL^{-1} after 40 days' test. On the contrary, the microfiltration treated mulberry wine samples remained sterilized since no bacterium was detected at all during the test. The results indicate that microfiltration had a prominent effect on mulberry wine, which could effectively extend the shelf life and guarantee better quality of product.

4. Conclusion

In this work, four different widely-used commercial membranes, of two different materials (PES, PVDF) and two different nominal pore sizes (0.22 μm and 0.45 μm) were employed to perform microfiltration of mulberry wine. Cake formation, mainly consisting of protein and polysaccharides, was the dominant mechanism during steady state of such process, independently on the membrane property. Fouling in this process was mainly reversible. Microfiltration was able to deliver a superior clarity, highly polydisperse and light-color mulberry wine with a satisfactory sterilization stability and well preserve the main basic properties and organic acid contents while induced certain loss of volatile compounds, especially esters and alcohols. Pore size indeed influenced the particle mean size and polydispersity of permeate, while the loss of volatile compounds depended on a complex combination of membrane material and pore size. This is the first time that the process of mulberry wine microfiltration has been systematically evaluated from the aspects of both fouling mechanism and permeate quality, providing guidance for the further development of mulberry wine production.

Conflicts of interest

There are no conflicts of interest to declare.

Acknowledgements

This work was sponsored by the Fundamental Research Funds for the Central Universities of China (Grant number: YJ201835), Sichuan university-Luzhou cooperation project (Grant number: 2017CDLZ-S18) and National Science Foundation of China (Grant number: 21978175).

References

1 W. Tchabo, Y. Ma, E. Kwaw, H. Zhang, X. Li and N. A. Afoakwah, *Food Bioprocess Technol.*, 2017, **10**, 1210–1223.
2 Y. You, X. Yuan, H. J. Lee, W. Huang, W. Jin and J. Zhan, *Food Funct.*, 2015, **6**, 401–408.
3 W. Tchabo, Y. Ma, E. Kwaw, H. Zhang, L. Xiao and M. T. Apaliya, *Food Chem.*, 2018, **239**, 470–477.
4 S. Liu, C. Wu, G. Fan, T. Li, R. Ying and Y. Miao, *J. Food Biochem.*, 2017, **41**, e12409.
5 X. Ouyang, B. Zhu, R. Liu, Q. Gao, G. Lin, J. Wu, Z. Hu and B. Zhang, *J. Food Process. Preserv.*, 2018, **42**, e13432.
6 L. Wang, X. Sun, F. Li, D. Yu, X. Liu, W. Huang and J. Zhan, *J. Funct. Foods*, 2015, **18**, 254–265.
7 S. Liu, E. Liu, B. Zhu, B. Chai, R. Liu, Q. Gao and B. Zhang, *J. Inst. Brew.*, 2018, **124**, 45–56.
8 W. Tchabo, Y. Ma, E. Kwaw, H. Zhang, L. Xiao and H. E. Tahir, *Food Chem.*, 2017, **232**, 89–97.
9 Y. El Rayess, C. Albasi, P. Bacchin, P. Taillandier, J. Raynal, M. Mietton-Peuchot and A. Devatine, *J. Membr. Sci.*, 2011, **382**, 1–19.
10 Y. E. Rayess, Y. Manon, N. Jitariouk, C. Albasi, M. M. Peuchot, A. Devatine and L. Fillaudeau, *J. Membr. Sci.*, 2016, **513**, 47–57.
11 A. Vernhet, D. Cartalade and M. Moutounet, *J. Membr. Sci.*, 2003, **211**, 357–370.
12 W. Zhang and F. Jiang, *Water Res.*, 2019, **157**, 445–453.
13 W. Chen, J. Mo, X. Du, Z. Zhang and W. Zhang, *Water Res.*, 2019, **151**, 243–251.
14 M. Ulbricht, W. Ansorge, I. Danielzik, M. König and O. Schuster, *Sep. Purif. Technol.*, 2009, **68**, 335–342.
15 I. Khalifa, W. Zhu, K. Li and C. Li, *J. Funct. Foods*, 2018, **40**, 28–43.
16 S. Ercisli and E. Orhan, *Food Chem.*, 2007, **103**, 1380–1384.
17 Q. Yuan and L. Zhao, *J. Agric. Food Chem.*, 2017, **65**, 10383–10394.
18 T. M. Gomes, I. M. Toaldo, I. C. da S. Haas, V. M. Burin, V. Caliari, A. S. Luna, J. S. de Gois and M. T. Bordignon-Luiz, *J. Funct. Foods*, 2019, **52**, 699–708.
19 Y. Jin, N. Hengl, S. Baup, G. Maitrejean and F. Pignon, *J. Membr. Sci.*, 2017, **528**, 34–45.
20 J. Teng, L. Shen, Y. He, B.-Q. Liao, G. Wu and H. Lin, *Chemosphere*, 2018, **210**, 769–778.
21 Y. Jin, N. Hengl, S. Baup, F. Pignon, N. Gondrexon, M. Sztucki, G. Gésan-Guiziou, A. Magnin, M. Abyan, M. Karrouch and D. Blésès, *J. Membr. Sci.*, 2014, **470**, 205–218.
22 H. Guo, J. Huang, R. Zhou, C. Wu and Y. Jin, *RSC Adv.*, 2019, **9**, 2928–2940.
23 A. L. Lim and R. Bai, *J. Membr. Sci.*, 2003, **216**, 279–290.
24 M. Li, Y. Zhao, S. Zhou and W. Xing, *Desalination*, 2010, **256**, 166–173.
25 M. Li, Y. Zhao, S. Zhou, W. Xing and F.-S. Wong, *J. Membr. Sci.*, 2007, **299**, 122–129.
26 R. Sondhi, Y. S. Lin and F. Alvarez, *J. Membr. Sci.*, 2000, **174**, 111–122.
27 V. L. Singleton, R. Orthofer and R. M. Lamuela-Raventos, in *Oxidants and Antioxidants, Pt A*, ed. L. Packer, Elsevier Academic Press Inc, San Diego, 1999, vol. 299, pp. 152–178.
28 Z. M. Sharif, M. S. Othman and N. J. Jalil, *AIP Conf. Proc.*, 2018, 020082.
29 L. Zhang, J. Huang, R. Zhou and C. Wu, *Int. J. Food Microbiol.*, 2017, **255**, 42–50.
30 X. Ding, C. Wu, J. Huang and R. Zhou, *LWT–Food Sci. Technol.*, 2016, **66**, 124–133.
31 Y. Jin, D. Li, M. Ai, Q. Tang, J. Huang, X. Ding, C. Wu and R. Zhou, *Food Res. Int.*, 2019, **121**, 422–432.

32 P. Nallasamy and S. Mohan, *Indian J. Pure Appl. Phys.*, 2005, **43**, 821–827.
33 F. Zhao, H. Chu, X. Tan, L. Yang, Y. Su, X. Zhou, J. Zhao and Y. Zhang, *J. Membr. Sci.*, 2016, **517**, 30–38.
34 V. Ivanova-Petropulos, Z. Nace Va, V. Sand Or, L. Maksz In, L. Na Gy, B. Berki Cs, T. Stafilov and F. Kilar, *Electrophoresis*, 2018, **39**, 1597–1605.
35 N. Markkinen, O. Laaksonen, R. Nahku, R. Kuldjärv and B. Yang, *Food Chem.*, 2019, **286**, 204–215.
36 C. Juan, K. Jianquan, T. Junni, C. Zijian and L. Ji, *J. Food Sci.*, 2012, **77**, C430–C436.